基于数学建模的铝合金双脉冲 MIG焊专家数据库设计

陈小峰， 林 放， 魏仲华， 薛家祥
（华南理工大学 机械与汽车工程学院，广州 510640）

摘 要：研制基于 DSP的数字化双脉冲 MIG焊电源，建立并论证了双脉冲 MIG焊波形的定频模型和变频模型. 结果表明，从 50～300 A电流范围内实现了精确到 1 A的双脉冲焊铝. 专家数据库设计以调节强弱脉冲群中脉冲个数为主、脉冲基值为辅，一方面实现了焊接电流的连续性可调，另一方面达到了焊接过程中小电流细调、大电流粗调的“人性化”效果. 在变频条件下保证其具有同等、连续的可调电流范围，通过调频可以得到理想疏密程度的鱼鳞纹焊缝. 焊接电流波形规整稳定，无断弧现象发生，基本无飞溅，焊缝呈美观、清晰的鱼鳞纹.

关键词：双脉冲参数建模；专家数据库；低频变频
中图分类号：TG434.5 文献标识码：A 文章编号：0253－360X(2011)05－0037－04

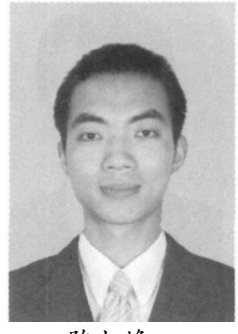
陈小峰

0 序 言

近年来，在机械制造领域，铝焊结构代替钢结构已经成为一种趋势. 同时，随着中国高铁和动车组的兴建和发展，铁路运输部门将需要大量的高速列车，铝合金将是建造高速列车的最佳原料之一，焊接技术作为铝合金的加工制造技术而成为关键[1].

双脉冲 MIG焊是一种焊接质量很高的熔化极焊接方法，母材热输入低，焊接变形小，能产生美观、高质量的鱼鳞纹焊缝，同时增强对熔池的搅拌振动，减少和消除焊缝气孔，从而获得致密的组织[2]. 但是双脉冲 MIG焊方法焊接工艺参数较多，如强弱脉冲群的基值、峰值电流的大小和时间，低频频率和占空比，送丝速度和焊接速度等，均直接影响焊接过程的稳定性和焊缝成形. 由于铝对焊接参数匹配要求很高，选择不当极易导致焊接效果急剧恶化. 如何合理匹配好各项参数，形成一元化调节的专家数据库，无疑给开发人员带来了巨大的挑战.

奥地利的 Fronius公司在焊接专家数据库领域极为出色，已开发出一系列带有多种专家数据库的数字化脉冲 MIG/MAG焊机[3]，这类高端焊机售价高昂，其核心就是不断升级的多种焊材的专家数据库[4]. 中国在高端机上的制造和科研水平落后于发达国家，重要工程中大量进口 Fronius和 OTC等国外产商的高端焊机设备. 据悉，2009年 Fronius在中国大陆销售额超过两亿人民币.

若能通过数学建模和工艺试验检验，调试出各个参数的最佳匹配关系，生成连续性可调的一元化专家数据库，对于深化双脉冲 MIG焊理论、提高国内企业自主研发高端焊机具有重要意义.

1 设计选取双脉冲重要参数

通常情况下，一脉一滴（ODPP)被认为是脉冲焊的最佳状态，而在实际生产过程中发现，射滴过渡的焊接状态也能产生高质量的焊缝[5]. 由于铝的一脉一滴范围比较宽，故暂不区分一脉一滴与射滴过渡区域. 双脉冲 MIG焊根据参数的不同匹配有多种方式来实现对熔滴过渡的控制，首要前提是保证对单位脉冲能量精准控制以实现一脉一滴或射滴.

日本 OTC公司的仝红军等人[6]通过试验得出直径为 1.2 mm铝镁合金焊丝 A5183单位脉冲强度和熔滴过渡形式的关系. 并因此提出了一个重要观点，铝的一脉一滴脉冲范围比较宽，这是铝的一个特点. 基于此理论，从而为文中试验在调节配置双脉冲参数过程提供了依据.

试验选取脉冲峰值时间为 2 ms，峰值电流为 250 A，选取的参数在一脉一滴曲线之上同时又靠近

收稿日期：2010－10－12
基金项目：国家自然科学基金资助项目（50875088）；广东省科技攻关项目（2010B010700001）；番禺区攻关项目（2010-Z-22-1）；黄埔区攻关项目（1021）.

一脉一滴曲线,从而保证实现一脉一滴.

试验设计建立在一个固定低频频率,通过改变送丝机上的电流给定大小,自动匹配双脉冲 MIG焊专家数据库的各项参数,达到控制焊接电流范围(50~300 A)连续性可调并实现稳定焊接的目的.

2 双脉冲 MIG焊数据库数学建模

2.1 定频双脉冲参数数学建模

为便于计算举例,假设双脉冲低频频率 f=3.3 Hz,则 $t_1=t_2=T/2=500/3.3$ ms,t_1、t_2分别为一个脉冲群周期内的强脉冲群时间、弱脉冲群时间. 图 1为双脉冲焊接电流波形.

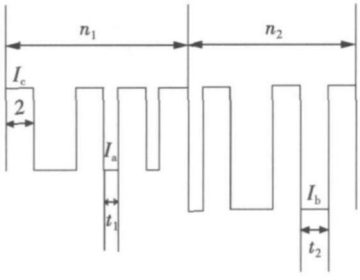

图 1 双脉冲焊接电流波形

Fig. 1 Current waveform of double pulse welding

由图 1所示,t_1、t_2分别为强脉冲群、弱脉冲群的基值时间,n_1、n_2分别为强脉冲群、弱脉冲群中脉冲的个数,I_a、I_b、I_c分别为强脉冲群基值电流大小,弱脉冲群基值电流大小,峰值电流大小,单位脉冲时间取 2 ms,可得

$$2n_1+t_1n_1=500/3.3 \tag{1}$$

$$2n_2+t_2n_2=500/3.3 \tag{2}$$

$$I=3.3[(2I_a+I_c t_a)n_1+(2I_a+I_b t_2)n_2] \tag{3}$$

式中:I为平均电流.

综合式(1)、式(2)、式(3),可得

$$I=500\left(\frac{2I_a+I_c t_a}{2+t_1}+\frac{2I_a+I_b t_2}{2+t_2}\right) \tag{4}$$

由式(4)可知,在 I_a、I_b、I_c固定的条件下,t_1、t_2决定了焊接电流大小. 但是,由于 t_1、t_2在波形采集以及反馈读取上存在不直观和视觉误差等问题,加大了设计难度. 从式(1)和式(2)中可知 n_1、n_2与 t_1、t_2存在一一对应的关系,同时 n_1、n_2在波形反馈读取上方便直观且均为整数,由此可大大提高运算效率,同时简化了编程过程和增强了程序的可读性. 因此,试验选取 n_1、n_2作为连续性可调电流的自变量.

为满足电流逐渐增大的目标,可以设定 n_1、n_2逐渐加大,则从式(1)和式(2)显而易见 t_1、t_2逐渐减小,取电流的子函数 $f(x)$为

$$f(x)=\frac{2I_a+mx}{2+x} \tag{5}$$

式中:m为 I_b或 I_c均小于 I_a,则

$$f'(x)=\frac{2(I_a-m)}{(2+x)^4}>0 \tag{6}$$

随着 x逐渐减小,$f'(x)$也逐渐变小,即电流子函数 $f(x)$斜率逐渐变陡,电流 I类似 $f(x)$与基值时间 t_b关系如图 2所示.

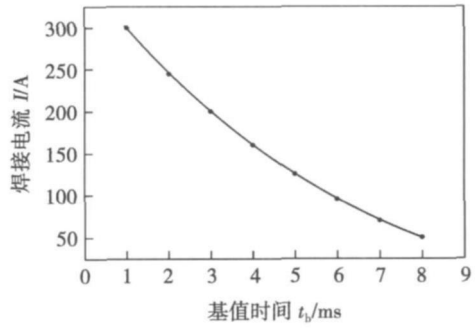

图 2 焊接电流与基值时间的关系曲线

Fig. 2 Relation curve of welding current and base time

通过合理给定强弱脉冲个数 n_1、n_2的初始值,按照一定规律逐步加大 n_1、n_2,则相对应 t_1、t_2逐步减小,从而导致电流逐步增大,并且电流增大速度逐渐加快. 基于此模型,理论实现了焊接电流的连续性可调,且达到小电流细调、大电流粗调的人性化调节目的. 从而论证了开发定频条件下铝合金双脉冲 MIG焊专家数据库的可行性.

2.2 变频双脉冲参数数学建模

上节论述了在定频条件下如何建立双脉冲数据库的数学模型,然而,要达到成熟、系统、产品化的专家数据库的要求,变频技术的应用是产品走向高端焊机的必由之路. 保持一定焊接速度,通过改变双脉冲低频频率,在得到高质量焊缝的同时可以调节鱼鳞纹焊缝的宽度,满足不同客户的实际生产需求.

假设用户所需要的低频频率为 f,其余双脉冲参数定义同 2.1小节,进行类似推导可得与式(4)完全一致的焊接电流公式. 在双脉冲波形其它参数不变的情况下,频率的改变并不影响电流大小.

由此可得结论,双脉冲低频频率的调节并不影响可调电流范围,从而为变频技术的推广使用实现了可能. 在变频技术的参数设计方面,参照 2.1小节可设计出用户所需低频频率的焊接电流.

3　双脉冲 MIG焊试验结果与分析

3.1　双脉冲参数优化

试验选取脉冲时间为 2 ms,脉冲电流为 250 A.通过一定的规律调节 n_1, n_2可实现电流从小到大阶梯跳跃式变化,但不能实现电流大小的连续性变化,如图 3所示. 同时随着脉冲个数 n_1, n_2增大到一定数目,脉冲个数比较密集,在低频频率固定的条件下,通过继续增加脉冲个数来增加电流是一件困难的事情.

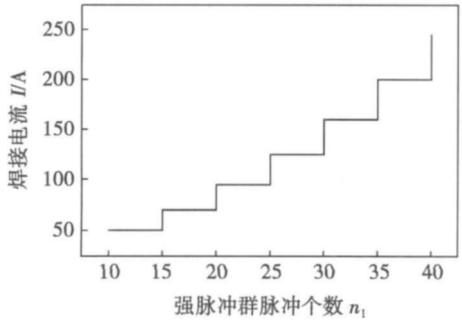

图 3　无基值协调焊接电流和脉冲个数变化曲线

Fig. 3　Relation curve of welding current and number of pluses without base current coordinated

为解决此困难,试验基于脉冲群的基值电流 I_j, I_j按照一定规律进行连续性可调节变化,辅助调节脉冲个数 n_1, n_2变化,有效地扩展焊接电流范围,从而实现了较宽范围连续可调焊接电流的目的,如图 4所示.

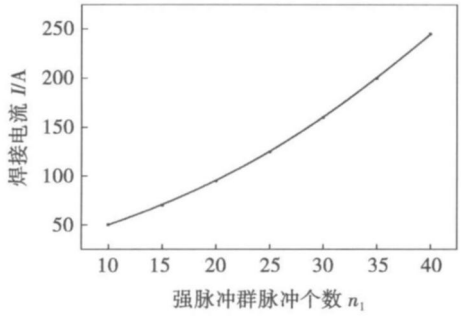

图 4　加基值协调焊接电流和脉冲个数变化曲线

Fig. 4　Relation curve of welding current and number of pluses with base current coordinated

3.2　试验条件

试验采用实验室研制的多功能数字化焊机,烧录自行设计基于定频模型下的专家数据库程序. 其中,双脉冲低频频率为 2.5 Hz,焊接电流范围为 50~300 A.试件尺寸为 2~12 mm纯铝板,采用 ϕ1.2 mm 1070纯铝焊丝,保护气体为 99.99%高纯氩气,气体流量为 15 L/min,焊丝伸出长度为 12 mm,平板堆焊.

3.3　试验结果及讨论

试验采用焊接电弧动态小波分析仪采集焊接过程的电压、电流波形,并经小波滤波后显示 U-I图. 经过大量试验测定,从小到大渐次旋转电流给定旋钮,双脉冲焊接电流可覆盖 50~300 A并精确到 1 A的所有电流,从而证实了该数据库精确程度满足实际生产要求.

图 5为 $n_1=10$, $n_2=0$条件下电流波形和焊缝宏观形貌, $I=58$ A.图 6为 $n_1=40$, $n_2=20$条件下电流波形和焊缝宏观形貌, $I=150$ A.图 7为焊接电流为 150 A对应的小波滤波 U-I图.

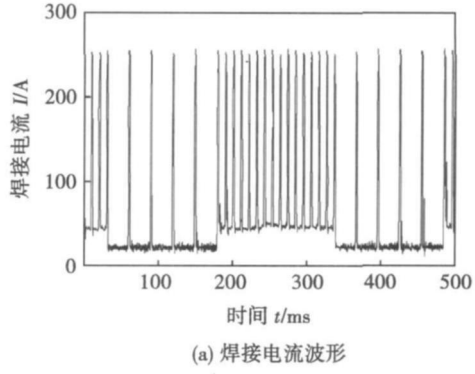

(a) 焊接电流波形

(b) 焊缝宏观形貌

图 5　$n_1=10$, $n_2=0$时的焊接电流波形和焊缝宏观形貌

Fig. 5　Current waveform and welding shape when $n_1=10$, $n_2=0$

在此方案下进行多次不同电流的试验. 结果表明,焊接电流规整稳定,焊接过程中,焊丝伸缩节奏稳定,低频噪声柔和,无断弧现象. 从图 5a和图 6a也可看出,采集的焊接电流波形稳定,动特性好. 从图 7可看出 U-I图比较规则,重复性好,表明焊接过程电弧特性较好. 从图 5b和图 6b可以看出焊缝基本不存在飞溅、咬边现象,焊缝呈现出均匀美观、纹路清晰的鱼鳞纹状. 值得一提的是,该设计方案下的小电流范围(50~110 A)可做到完全无飞溅,焊缝色泽光亮,焊接效果很好.

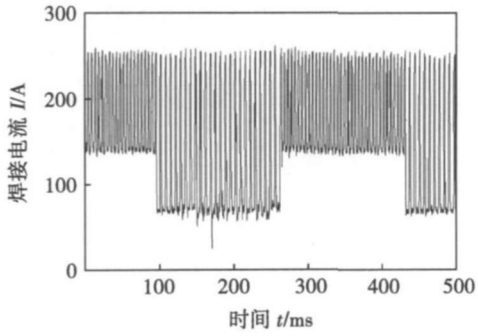

(a) 焊接电流波形

(b) 焊缝宏观形貌

图 6 $n_1=40, n_2=20$ 时焊接电流波形和焊缝宏观形貌

Fig. 6 Current waveform and welding shape when $n_1=40, n_2=20$

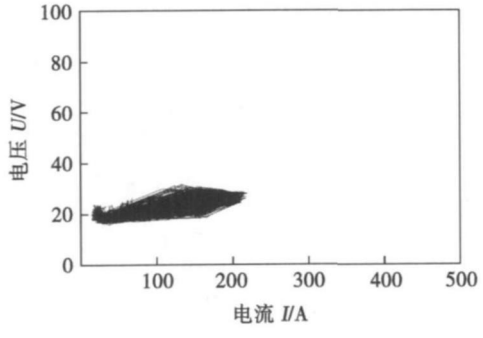

图 7 $I=150$ A 条件下的 U-I 图

Fig. 7 U-I curve when $I=150$ A

4 结 论

(1)建立双脉冲 MIG焊波形的定频模型和变频模型,并论证了开发此模型下专家数据库的可行性.

(2)在双脉冲 MIG焊专家数据库开发中以调节强弱脉冲群脉冲个数为主、强弱脉冲群基值为辅,在连续性可调焊接电流大小的基础上达到焊接过程中小电流细调、大电流快调的人性化效果.

(3)变频条件下依然具有同等、连续性可调的电流范围,适合焊接工作人员根据具体焊接状态得到理想疏密度的鱼鳞纹焊缝,增加了产品的经济附加值.

(4)文中数学建模方法适用于开发多种不同丝径、不同材质的专家数据库,实现一元化调节的功能.

参考文献:

[1] Kuagai S, Recent technolpgical developments in welding of aluminum and its alloys[J]. Journal of Japan Welding Society, 2002, 71(5): 109—114.

[2] Subramanima B S, White D R. Experimental approach to selection of pulsing parameters in pulsed GMAW[J]. Welding Journal, 1999, 66(5): 166—172.

[3] 马 德, 殷树言, 刘 嘉, 等. 脉冲 MIG焊铝工艺特性的研究[J]. 电焊机, 2004, 34(5): 44—46.
Ma De, Yin Shuyan, Liu Jia, et al. Study of aluminum PMIG process[J]. Electric Welding Machine, 2004, 34(5): 44—46.

[4] Hirata Y. Pulse arc welding[J]. Journal of Japan Welding Society, 2002, 71(3): 115—130.

[5] Palani P K, Murugan N. Selection of parameters of pulsed current gas metal arc welding[J]. Journal of Materials Processing Technology, 2006, 172(1): 1—10.

[6] 仝红军, 上山智之. 低频调制型脉冲 MIG焊接方法的工艺特点[J]. 焊接, 2001(11): 33—35.
Tong Hongjun, Ueyama Tomoyuki. Features of low frequency modulated type pulsed MIG welding process[J]. Welding & Joining, 2001(11): 33—35.

作者简介:陈小峰,男,1984年出生,硕士.主要从事多功能数字化焊机研发工作.发表论文 5篇. Email: xiaoshan35@163.com

100084, China; 2. Key Laboratory for Advanced Materials Processing Technology, The Ministry of Education, Tsinghua University, Beijing 100084, China). p. 17—20, 24

Abstract: The effects of welding parameters including laser power, welding speed, welding conditions on pore formation tendency (represented as porosity) during laser welding of die-cast magnesium alloys with two different gas contents were investigated, and the porosity prevention measures were also studied. It is shown that the pore formation tendency during laser welding of 2 mm thick die-cast magnesium alloys with higher gas content is greater than that of 5 mm thick die-cast magnesium alloys with lower gas content. As a whole, the porosity increases with the increase of laser power and the decrease of welding speed for both two thicknesses. For 5 mm thick die-cast magnesium alloys with lower gas content, low porosity weld bead can be obtained by both double sided welding and remelting after welding, and the porosity can reduce to 2.4% and 2.5%, respectively. However, for the 2 mm thick die-cast magnesium alloys, these porosity prevention measures are not effective.

Key words: pore; pore prevention; laser welding; welding parameters; die-cast magnesium alloys

Effect of high-energy shot peening on diffusion behavior of nickel in iron. WANG Yuetian, SHENG Guangmin, SUN Jianchun, LU Hao (School of Materials Science and Engineering, Chongqing University, Chongqing 400030, China). p. 21—24

Abstract: High-energy shot peening (HESP) was used to make surface self nano-crystallization (SSNC) on pure iron. The thickness of the deformation layer, surface grain size and hardness were characterized by optical microscope (OM), scanning electron microscopy (SEM) and X-ray diffraction analysis (XRD), and then Ni film was penetrated into the surface of iron by the Gleeble-1500 thermal simulation test machine. The SEM was used to compare the diffusion effects. The results showed that the surface of industrial pure iron was refined obviously after the shot peening treatment, its hardness increased significantly and was one time higher than that of the matrix. Under the same conditions, the diffusion rate of Ni in the specimen after SSNC was higher than that without SSNC, so the SSNC technology can improve diffusion effect of Ni on the surface of industry pure iron.

Key words: pure iron; SSNC; shot peening; diffusion

Signal processing in ultrasonic test of austenitic welds based on time-frequency analysis. WANG Bingfang, HAN Zandong, YUAN Keyi, CHEN Yifang (Key Laboratory for Advanced Materials Processing Technology, The Ministry of Education, Tsinghua University, Beijing 100084, China). p. 25—28

Abstract: Signal processing in ultrasonic test of austenitic welds was studied. Based on time-frequency analysis, a comprehensive signal processing method was proposed, which was a combination of matching pursuit and wavelet analysis. This method distinguishes flaw information and material noise from a point of energy and frequency respectively, and improves the SNR of the ultrasonic echo signal. To verify the effectiveness of the method, an ultrasonic test system was established. Test experiment was carried out with a 53 mm thick weld specimen, and a signal with large amount of material noise was acquired. The noised signal was processed by the proposed method. The first 18 time-frequency atoms were extracted by matching pursuit with sym8 wavelet packet dictionary, the extracted signal was analyzed by sym8 wavelet decomposition and reconstructed with low frequency coefficients. The result shows that the material noise is reduced effectively and the flaw echo signal is enhanced significantly.

Key words: austenitic welds; ultrasonic test; time-frequency analysis; matching pursuit; wavelet analysis

Analysis on growth mechanism on interfacial interlayer on Fe/Al couple. WU Mingfang[1,2], SI Naichao[1], WANG Jing[1], WANG Fengjiang[1] (1. School of Materials Science and Engineering, Jiangsu University, Zhenjiang 212013, China; 2. School of Materials Science and Engineering, Jiangsu University of Science and Technology, Zhenjiang 212003). p. 29—32

Abstract: To understand the formation mechanism and growth behavior of Fe-Al intermetallics, the element diffusion and interfacial reactive interlayer in Fe/Al couple were studied at the different heating temperature and holding time. The interfacial structure is Fe/FeAl$_x$+Al/FeAl/Al at the shorter holding time, while the unstable FeAl$_x$ and FeAl will change into the stable Fe$_2$Al$_5$ and FeAl$_3$ intermetallics at a longer holding time. The final interfacial structure was Fe/Fe$_2$Al$_5$+FeAl$_3$/Al. The growth of interfacial reactive layer follows the parabolic rule, and its rate is controlled by the diffusion rate of Fe atoms into Al side. The results are helpful to improve the bonding quality between aluminum alloys and stainless steel.

Key words: Fe-Al; diffusion; interfacial structure

Investigation of out-of-plane welding distortion in aluminum alloy welding with external restraint. XIAO Xiaoming, PENG Yun, ZHANG Jianxun, PEI Yi, TIAN Zhiling (1. State Key Laboratory of Advanced Steel Processes and Products, Central Iron & Steel Research Institute, Beijing 100081, China; 2. State Key Laboratory for Mechanical Behavior of Materials, Xi'an Jiaotong University, Xi'an 710049, China). p. 33—36

Abstract: The characteristics of constraint force and dynamic welding distortion of aluminum alloy 5A12 with constraint TIG welding were investigated by dynamic temperature and distortion measuring system. The effects of constraint force and its release on out-of-plane welding distortion were analyzed. Research results show that out-of-plane welding distortion is different with the different constraint force, and welding distortion can be controlled by the proper constraint force; the welding distortion will rebound to some extent after the constraint force being released, which is the main factor to result in the residual distortion of constraint welding; the residual distortion of 6 mm thick aluminum alloy 5A12 plate can be well restrained at the constraint force of 0.2 kN, and the loading position is 45 mm form the centerline of weld.

Key words: aluminum alloy; deformation; constraint force; elastic recovery

Double-pulsed MIG expert database based on mathematical modeling. CHEN Xiaofeng, LIN Fang, WEI Zhonghua, XUE Jiaxiang (School of Mechanical & Automotive Engineering, South China University of Technology, Guangzhou 510640, China). p. 37—40

Abstract: Double-pulsed gas metal arc welding machine was developed based on both static-frequency and dynamic-frequency models. The feasibility of the models was proved and an expert database was developped based on welding experiments. The results indicate that the accuracy can be guaranteed to 1 A for the current range 50—300 A of double-pulsed welding of Al continuous adjustments can be achieved by adjusting dominant role of the number of pulses and the subsidiary role of the base-current value. Moreover, by using this method, the current can be adjusted slowly for low welding current and rapidly for high welding current. The adjusting range of welding current can be kept constant and continuous for the dynamic-frequency mode. The fish scale pattern weld with proper density scaly can be obtained by adjusting the modulation frequency. The welding currents are kept stable and there is interruption arc and little spatter, the welding seams are beautiful.

Key words: double-pulsed; modeling; expert database; dynamic-frequency

Analysis on failure modes of AZ31B magnesium alloy joint of resistance spot welding ... AO Sansan[1,2], LUO Zhen[1,2], BU Xianzheng[1,2], WAND Rui[1,2] (1. School of Materials Science and Engineering, Tianjin University, Tianjin 300072, China; 2. Tianjin Key Laboratory of Advanced Joining Technology, Tianjin University, Tianjin 300072, China). p. 41—44, 48

Abstract: The fracture mechanics theory was used to analyze the two fracture modes in shear tension tests for AZ31B magnesium alloy joint of resistance spot welding. The shear tension test results showed that the fracture mode of the AZ31B magnesium was influenced by the maximum tensile stress at the nugget boundary. The button-pullout fracture will happen if the maximum tensile stress at the nugget boundary is lower than the tensile strength of the base metal; otherwise the interfacial fracture happens. And there is a critical nugget diameter when the failure mode is transferred from button-pullout fracture to interfacial fracture. If the nugget diameter is less than 6.5 mm, the button-pullout fracture will occur and the interfacial fracture will happen if the nugget diameter is larger than 6.5 mm. The calculation on the equivalent stress intensity factor at the spot weld indicates that the interfacial fracture is harder to occur with the stress intensity factor being increased, and the fracture mode has little influence on the load-capacity of the joint.

Key words: AZ31B magnesium alloy; resistance spot welding; stress intensity factor; fracture mode

Automatic offset correction system of narrow gap arc welding torch for rail ... LIU Zhengwen, ZHENG Jun, JI Guanyu, ZHU Zhiming, PAN Jiluan (1. Department of Mechanical Engineering, Tsinghua University, Beijing 100084, China; 2. Beijing Jinglonghua Science and Technology Development Ltd. Co., Beijing 100038, China). p. 45—48

Abstract: Automatic narrow-gap arc welding can be used in rail welding. By oscillating and moving the bacilliform welding torch, it can join together the rails by fusing two side walls of groove. While the swinging torch control is open-loop control, which can lead to the accumulated swing error. In order to decrease the error, a double CCD visual sensor system was used to observe the welding pool for the existing equipments and rail seam arc welding techniques. And then it calculates the position offset and oscillating angle offset of the welding wire can be calculated in real time to control the torch movement. The results show that the proposed method can effectively reduce both the position offset and the oscillating angle offset, and avoid welding defect.

Key words: rail; arc welding; oscillating control of welding torch; CCD visual sensor; image processing

A new approach to measure deviation of seam tracking in high-power fiber laser welding ... GAO Xiangdong, YOU Deyong, KATAYAMA Seiji (1. School of Mechanical and Electrical Engineering, Guangdong University of Technology, Guangzhou 510006, China; 2. Joining and Welding Research Institute, Osaka University, Osaka 567-0047, Japan). p. 49—52

Abstract: A new approach to measure the deviation of seam tracking was proposed based on near-infrared image processing and recognition during high-power fiber laser welding. The molten pool images were acquired by a high speed camera with the narrow bandpass filters. Based on the gray distribution of the near-infrared image of the molten pool, its temperature distribution parameter was defined as the measured eigenvalue of seam tracking. A near-infrared image model was established to measure the deviation between the welding seam and the laser beam focus in real time by using the least square algorithm. The effectiveness of the proposed approach was verified by the welding experiments.

Key words: high-power fiber laser welding; seam tracking; near-infrared image; deviation measuring

Finite element analysis on reliability of indium soldered joint in infrared focal plane array detector ... MENG Qingduan[1,2], LÜ Yanqiu[1], LU Zhengxiong, SUN Weiguo[2] (1. School of Electronic and Informational Engineering, Henan University of Science and Technology, Luoyang 471003, China; 2. Luoyang Optoelectro Technology Development Center, Luoyang 471009, China). p. 53—56

Abstract: Based on viscoplastic model, the reliability of indium sphere soldered joint in infrared focal plane array detector was analyzed by finite element method. Simulation results show that the maximum equivalent stress appears on the contact area between InSb chip and indium sphere, which is located in the corner of indium sphere array and far away from the symmetric center of the detector. When the infrared detector was loaded periodically with temperature cycles, the maximal stress also varied periodically. As the temperature decreases from the room temperature to 77 K, the maximal stress increases rapidly to the maximum value, and during the holding time, the stress relaxation phenomena appears, and as the temperature increases, the maximal stress reduces sharply. As the diameter of the indium sphere increases, the maximum stress varies irregularly, while the plastic energy analysis results show that as the diameters of indium sphere increase, its plastic work decreases, and its plastic energy accumulation also reduces, which indicates that the structure with larger diameter has the higher fatigue reliability. It is noticed that when the diameter of the indium solder is set to be 30 μm, the stress distribution on all the contacting areas is uniform and concentrated, and the stress is the lowest.

Key words: flip chip; finite element method; viscoplas-